Proceedings of the Combustion Institute SAND2020-1363C

# Direct numerical simulation of turbulent boundary layer premixed combustion under auto-ignitive conditions

--Manuscript Draft--

| | |
|---|---|
| **Manuscript Number:** | PROCI-D-19-01753 |
| **Article Type:** | 12. Gas Turbine/Rocket Combustion |
| **Keywords:** | Direct numerical simulation; Flame-wall interactions; Auto-ignition; Flame propagation |
| **Corresponding Author:** | Haiou Wang<br>Zhejiang University<br>Hangzhou, CHINA |
| **First Author:** | Zhuo Wang |
| **Order of Authors:** | Zhuo Wang |
| | Haiou Wang |
| | Kun Luo |
| | Evatt R. Hawkes |
| | Jacqueline H. Chen |
| | Jianren Fan |
| **Abstract:** | In the present work, premixed combustion in turbulent boundary layer under auto-ignitive conditions is investigated using direct numerical simulation (DNS). The inflow of the reactive DNS is obtained by temporal sampling of a corresponding inert DNS of turbulent boundary layer at a location with $Re_\tau = 360$, where $Re_\tau$ is the friction Reynolds number. The reactants of the DNS are determined by mixing the products of lean natural gas combustion with a H2/N2 fuel jet, resulting in a lean mixture of high temperature with a short ignition delay time. In the free-stream the reaction front is stabilized at a streamwise location which can be predicted using the free-stream velocity $U_\infty$ and the ignition delay time $\tau_{ig}$. The combustion modes in various regions are examined with respect to the statistics of displacement velocity and the analysis of species budget. It is indicated that flame propagation prevails in the near-wall region and auto-ignition is increasingly important as the wall-normal distance increases. The interactions of turbulence and combustion are studied in terms of statistics of reaction front normal vector and strain rate tensors. It is found that the front normal preferentially aligns with the most compressive strain rate in regions where the effects of heat release on the strain rate are minor and with the most extensive strain rate where the effects are significant. Negative correlations between the wall heat flux and flame quenching distance are observed, and it was shown that heat release at the wall is evident. A new quenching mode, back-on quenching, is identified. Heat release rate at the wall is the highest when head-on quenching occurs and lowest when back-on quenching occurs. |

# Direct numerical simulation of turbulent boundary layer premixed combustion under auto-ignitive conditions

Zhuo Wang[a], Haiou Wang[a,*], Kun Luo[a], Evatt R. Hawkes[b,c], Jacqueline H. Chen[d], Jianren Fan[a]

[a]*State Key Laboratory of Clean Energy Utilization, Zhejiang University, Hangzhou 310027, PR China*
[b]*School of Manufacturing and Mechanical Engineering, University of New South Wales, Sydney, NSW, 2052, Australia*
[c]*School of Photovoltaics and Renewable Energy Engineering, University of New South Wales, Sydney, NSW, 2052, Australia*
[d]*Sandia National Laboratories, Livermore, CA 94550, USA*

## Abstract

In the present work, premixed combustion in turbulent boundary layer under auto-ignitive conditions is investigated using direct numerical simulation (DNS). The inflow of the reactive DNS is obtained by temporal sampling of a corresponding inert DNS of turbulent boundary layer at a location with $Re_\tau = 360$, where $Re_\tau$ is the friction Reynolds number. The reactants of the DNS are determined by mixing the products of lean natural gas combustion with a $H_2/N_2$ fuel jet, resulting in a lean mixture of high temperature with a short ignition delay time. In the free-stream the reaction front is stabilized at a streamwise location which can be predicted using the free-stream velocity $U_\infty$ and the ignition delay time $\tau_{ig}$. The combustion modes in various regions are examined with respect to the statistics of displacement velocity and the analysis of species budget. It is indicated that flame propagation prevails in

*Corresponding author: Haiou Wang
*Email address:* wanghaiou@zju.edu.cn (Haiou Wang)

the near-wall region and auto-ignition is increasingly important as the wall-normal distance increases. The interactions of turbulence and combustion are studied in terms of statistics of reaction front normal vector and strain rate tensors. It is found that the front normal preferentially aligns with the most compressive strain rate in regions where the effects of heat release on the strain rate are minor and with the most extensive strain rate where the effects are significant. Negative correlations between the wall heat flux and flame quenching distance are observed, and it was shown that heat release at the wall is evident. A new quenching mode, back-on quenching, is identified. Heat release rate at the wall is the highest when head-on quenching occurs and lowest when back-on quenching occurs.
*Keywords:* Direct numerical simulation, Flame-wall interactions, Auto-ignition, Flame propagation

---

## 1. Introduction

Turbulent wall-bounded combustion is widely encountered in many industrial applications, such as gas turbines, internal combustion engines and scramjets [1]. In these combustion equipment, the interactions between turbulence, combustion and the wall strongly affect the characteristics of combustion efficiency and pollutant emissions. Unfortunately, current understanding of these complex interactions is still unenough. Therefore, fundamental studies of turbulent combustion in wall-bounded flows are desirable.

Direct numerical simulation (DNS) is a useful tool to provide physical insights of turbulent wall-bounded combustion [2–8]. DNS of turbulent flame-wall interactions without shear flows was first conducted by Pointsot *et al.*

[2], and a model describing the interactions of turbulent premixed flames and walls was proposed. In practical combustion process, the flame-wall interactions are usually accomplished by strong shear flows such as channel or boundary layer flows. Bruneaux *et al.* [3] performed three-dimensional DNS of flame-wall interactions in a channel flow, and they found that the near-wall turbulence structures have a great influence on the flame quenching process. Gruber *et al.* [4] studied the evolution of a premixed V-shaped flame as well as its interaction with a wall in turbulent channel flows. DNS of oblique wall quenching in a turbulent V-shaped flame interacting with a wall was reported by Lai *et al.* [6]. Despite of the above DNS studies of turbulent wall-bounded combustion, to our best knowledge, there has been no work devoted to DNS of combustion in boundary layer turbulence.

In modern combustion techniques such as sequential combustion systems [9–12], fuel is mixed with hot gases produced by lean flames of the first stage, resulting in the second stage combustion which is under auto-ignitive conditions. The second stage flames could further interact with the wall and wall-bounded turbulence. It has been shown that the second stage is mainly stabilized by auto-ignition [9, 11], but flame propagation may also assist flame stabilization in regions with low flow velocities [13] or with heat loss to cold walls [12]. Complex combustion modes of auto-ignition and flame propagation are therefore expected in turbulent wall-bounded reactive flows, which deserves detailed investigations, particularly for premixed combustion in turbulent boundary layers.

Based on the above discussion, the objectives of the paper are as follows. First, DNS of premixed combustion in spatially developing boundary layer

turbulence under auto-ignitive conditions is performed. Second, the two combustion modes of auto-ignition and flame propagation are identified in various regions of the turbulent boundary layer. Finally, the complex interactions between boundary layer turbulence, combustion and wall are examined.

## 2. Simulation setup

A configuration of premixed combustion in turbulent boundary layers stabilized by auto-ignition is considered in the present work. The thermochemical conditions of the reactants are selected to be representative of those at the inlet of second stage combustion in heavy-duty gas turbines [14]. Particularly, the reactants are determined by adiabatically mixing the vitiated air (products of lean natural gas combustion in first stage combustion) and $H_2/N_2$ fuel jet in the experiment [10]. The resultant equivalence ratio of the reactants is 0.4 and the temperature is 1062 K. The composition of the resultant mixture is listed in Table 1. A 9 species and 19-step mechanism for $H_2$ combustion by Li *et al.* [15] is employed for the DNS. The mass fractions of $CO_2$ and $H_2O$ in the reactants are lumped together as $CO_2$ is not included in the mechanism for $H_2$ combustion. In order to facilitate the ignition process and make the DNS configuration more compact, the reactant temperature $T_\infty$ is increased to 1150 K. Based on the thermochemical conditions described above, the ignition delay time of the reactants $\tau_{ig}$ is 0.11 ms. The flow velocity of the main stream is $U_\infty = 100$ m/s. The ignition distance $L_{ig}$ evaluated as $L_{ig} = \tau_{ig} \cdot U_\infty$ is 11 mm. The wall temperature is set to $T_w = 750$K, consistent with the DNS of Aditya *et al.* [12].

A schematic of the DNS configuration is displayed in Fig. 1. The compu-

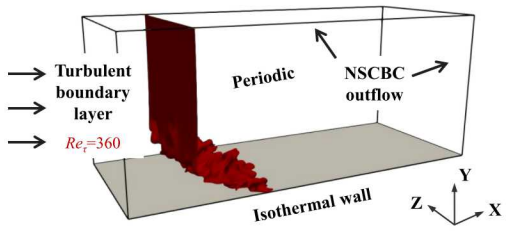


Figure 1: Schematic of the DNS configuration.

tational domain is a rectangular box with $L_x \times L_y \times L_z = 60 \times 25 \times 25$ mm$^3$, where $L_x$, $L_y$ and $L_z$ are the domain length in the streamwise, $x$, wall-normal, $y$, and spanwise, $z$, directions, respectively. The boundary conditions are non-reflecting in the streamwise direction and periodic in the spanwise direction. A fully developed boundary turbulent flow of reactants enters the domain at the inflow ($x = 0$) plane. No-slip isothermal wall ($y = 0$) and non-reflecting outflow ($y = L_y$) boundaries are used in the wall-normal direction. Fine grids near the wall are required to capture the near-wall turbulence and flame structures. The grids are stretched in the wall-normal direction with $\Delta y = 8.6$ $\mu$m at the wall. There are 3 points within $y^+ = 1$ and 24 points within $y^+ = 10$, where the superscript '+' denotes non-dimensionalization by the viscous length scale $\delta_v$ ($\delta_v = 21$ $\mu$m). In the streamwise direction, a uniform grid with a resolution of $\Delta x = 45.0$ $\mu$m ($\Delta x^+ = 2.2$) is set in the flame region of $0 \leq x \leq 2.0$ cm, and then it is stretched elsewhere. The grids are uniform in the spanwise direction, resulting in a grid size of $\Delta z = 45.5$ $\mu$m ($\Delta z^+ = 2.2$). Both the turbulence and flame structures can be resolved using the grids. The resultant grid number is $N_x \times N_y \times N_z = 1024 \times 600 \times 550$.

To obtain the boundary layer turbulence for the inflow of the reactive

Table 1: Mixture composition based on the experiment and that used in the DNS

| | $Y_{O_2}$ | $Y_{N_2}$ | $Y_{H_2O}$ | $Y_{CO_2}$ | $Y_{H_2}$ |
|---|---|---|---|---|---|
| Exp. | 0.1568 | 0.7649 | 0.0317 | 0.0388 | 0.0078 |
| DNS | 0.1568 | 0.7649 | 0.0705 | - | 0.0078 |

case, an auxiliary inert DNS was performed. The same configuration was used in the inert and reactive cases, except that the computational domain is much longer in the streamwise direction ($L'_x = 350$ mm) and the reactions are turned off in the inert case. To trigger the transition of the spatially developing boundary layer, a mean flow superimposed with an isotropic turbulent perturbation is used at the inlet in the near-wall region for the inert case. The velocity fluctuations imposed at the inlet of the reactive case are obtained by temporal sampling of the inert case at a certain plane in the streamwise direction with a friction Reynolds number $Re_\tau$ of 360, which corresponds to a streamwise location around $x = 300$ mm and a boundary layer thickness of $\delta_u = 7.4$ mm.

The validations of the inert DNS regarding the mean and fluctuating velocity statistics are provided. Since benchmark data of compressible boundary layer turbulence are rare due to difficulty in experimental measurements, it is common to compare with the equivalent data of incompressible boundary layer using the Morkovins hypothesis [17]. Figure 2 shows the distribution of van-Driest-transformed mean streamwise velocity $u^+_{VD}$ [18] and the density-scaled velocity variance and Reynolds stress component [19]. As can be seen, very good agreements between the present DNS and the reference incompressible DNS data with $Re_\tau = 360$ by Schlatter et al. [16] are obtained.

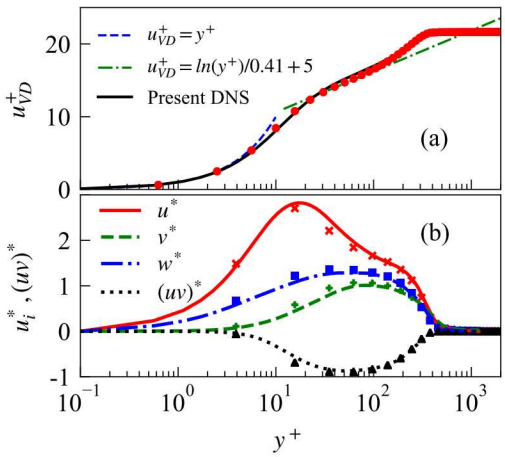


Figure 2: Distributions of (a) van-Driest-transformed mean streamwise velocity and (b) density-scaled velocity variance and Reynolds stress component. Symbols denote DNS data by Schlatter *et al.* [16].

Both the inert and reactive cases were performed using the DNS code S3D [20]. It solves the compressible Navier-Stokes equations including continuity, momenta, species mass fractions and total energy. The spatial derivatives are discretized using an eighth-order finite difference scheme. Time integration is achieved by a fourth-order six-stage Runge-Kutta method. A tenth-order spatial filter is applied to eliminate the high frequency oscillations [21]. The simulations advanced for more than $4t_j$ after the flame achieved a statistically steady state to collect stationary statistics, where $t_j$ is the flow-through time defined as $t_j = L_x/U_\infty$.

## 3. Results and discussion

In this section, the combustion modes in various regions are first examined, and the roles of auto-ignition and flame propagation are identified.

Then, the interactions of boundary layer turbulence and the reaction fronts are revealed. Finally, the flame/wall interactions for premixed combustion are investigated.

### *3.1. Combustion modes*

Figure 3 shows the distribution of mean heat release rate normalized by its maximum value. The averaging is performed in time and the spanwise direction. The mean reaction front position is marked by the iso-surface of $\bar{c} = 0.7$, where $c$ is the progress variable defined based on the mass fraction of hydrogen. Noted that the instantaneous iso-surface of $c = 0.7$ corresponds to the peak heat release rate position in the DNS (not shown). It can be seen that outside of the boundary layer the reaction front is anchored at a streamwise distance which equals to the ignition distance $L_{ig}$, while inside the boundary layer the front is bending downstream.

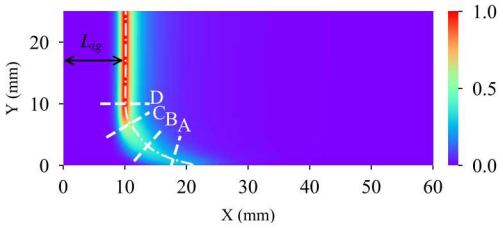


Figure 3: Contour of normalized mean heat release rate. The white dash-dotted line denotes the location of $\bar{c} = 0.7$.

Various regions of the reaction zones are selected for the combustion mode analysis. Four planes (*i.e.* plane A, plane B, plane C and plane D), which are perpendicular to the $\bar{c} = 0.7$ iso-surface, are identified in Fig. 3. The wall-normal distance of the intersections between planes A, B, C and D and the $\bar{c} = 0.7$ iso-surface is 1.0, 3.2, 6.8 and 10.0 mm, respectively. Plane

A is very close to the wall with a low flow velocity, while plane D is close to the free-stream where the flow velocity is very large. Since the DNS is statistically steady, the displacement speed $S_d$, which measures the speed of the reaction front relative to the flow, must be balanced by the flow velocity in the front normal direction $\mathbf{u} \cdot \mathbf{n}$ [22]. The reaction front normal vector is defined as $\mathbf{n} = -\nabla c/|\nabla c|$, and $\mathbf{n}$ points towards the reactant by convention. The displacement speed $S_d$ is defined as [23]:

$$S_d = \frac{1}{|\nabla c|}\frac{Dc}{Dt} = \frac{\dot{\omega}_c}{\rho|\nabla c|} + \frac{1}{\rho|\nabla c|}\frac{\partial}{\partial x_i}(\rho D_c \frac{\partial c}{\partial x_i}) \tag{1}$$

where $\dot{\omega}_c$ and $D_c$ are the reaction rate and diffusivity of the progress variable, respectively. The density-weighted displacement speed, $S_d^*$, is used to account for the thermal expansion effects across the front, which is calculated as $S_d^* = \rho S_d/\rho_u$, where $\rho_u$ is the density of unburned gas [22, 24, 25]. It is obvious that the magnitude of $S_d^*$ and $\mathbf{u} \cdot \mathbf{n}$ decreases with decreasing wall-normal distance for reactive flows in boundary layer turbulence. The statistics of the density-weighted displacement velocity are examined in the following.

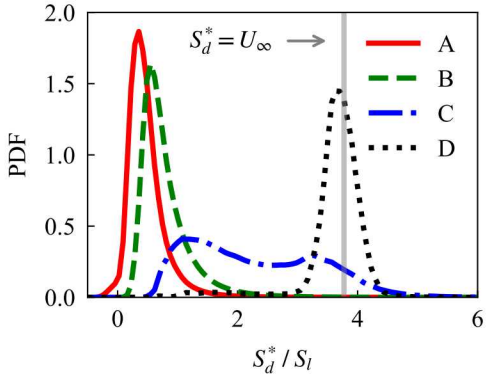


Figure 4: The PDF of density-weighted displacement speed nomralized by laminar flame speed in various regions conditioned on $c = 0.7$.

The probability density functions (PDFs) of $S_d^*$ normalized by $S_l$ in various regions conditioned on $c = 0.7$ are shown in Fig. 4. $S_l$ is the reference laminar flame speed. In combustion under auto-ignitive conditions, the identification of a reference laminar flame is challenging as the mixture ahead of the flame can auto-ignite. In the present work, the method described in [26] is employed to identify the reference laminar flame, and the corresponding laminar flame speed is $S_l = 26.5$ m/s. More details of the reference laminar flame are provided in the supplementary material. It is suggested that for local reaction fronts with a displacement velocity much larger than $S_l$, reaction is dominant over diffusion and auto-ignition plays an important role; while for those with a displacement velocity much smaller than $S_l$, diffusion is more significant, and propagating flames prevail. As can be seen from Fig. 4, the most probable value of the displacement speed at plane D is close to the free-stream velocity $U_\infty$, which is much larger than the reference laminar flame speed $S_l$. The reaction front is, therefore, mainly stabilized by auto-ignition. As the wall-normal distance of the reaction front decreases, the peak of the PDF shifts to lower values and flame propagation plays an increasingly important role. It is interesting to observe that the PDF for plane C has two peaks, indicating the co-existence of the two combustion modes.

The study of combustion modes is complemented with species budget analyses. Figure 5 presents the budget terms of H species conditioned in various regions on the distance function, $l$, which is defined such that at each point in the computational domain it signifies the shortest normal distance to the reaction front, computed by solving the Eikonal equation: $|\nabla l| = 1$.

The value of $l$ is set to zero at $c = 0.7$, and is negative in the reactants and positive in the products. The species H is selected as it represents an important species in hydrogen combustion. It is readily observed that the reaction term is balanced by the diffusion term at plane A, which confirms that flame propagation prevails in the near-wall region. As the wall-normal distance increases, the ratio of the reaction term to the diffusion term is increased, and auto-ignition is dominant. Therefore, consistent results are obtained with both the analyses of displacement velocity and species budget.

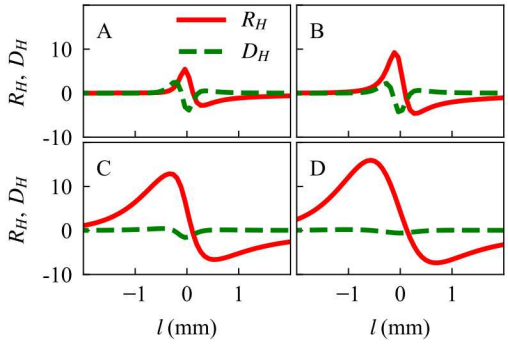


Figure 5: Budget terms of H in various regions conditioned on the distance function. $R_H$ is for the reaction term and $D_H$ is the diffusion term.

### *3.2. Interactions of turbulence and combustion*

Next, the statistics of reaction front normal and strain rate tensor are presented. Figure 6 shows the PDFs of the reaction front normal components in various regions conditioned on $c = 0.7$. As can be seen, the most probable value of $n_x$ at plane A is 0 and that of $n_y$ is -1, which implies that the reaction fronts propagate downwards in the near-wall region. As the wall-normal distance increases from plane A to plane D, the most probable value

of $n_x$ shifts from 0 to -1, so that the probability increases for the reaction front normal vector to point towards the inflow plane of $x = 0$. At plane D, the distributions of $n_x$, $n_y$ and $n_z$ are close to delta functions at -1, 0 and 0, respectively, *i.e.* the ignition front is essentially laminar at plane D.

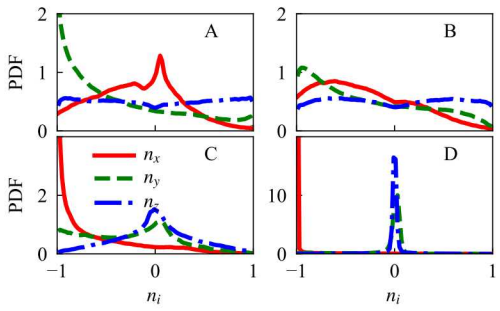


Figure 6: The PDFs of front normal components in various regions conditioned on $c = 0.7$.

Turbulence structures can be described in terms of the strain rate tensor $S_{ij}$, which is defined as $S_{ij} = 1/2(\partial u_i/\partial x_j + \partial u_j/\partial x_i)$. The three principal eigenvalues of $S_{ij}$ are $\lambda_1$, $\lambda_2$ and $\lambda_3$ with the convention $\lambda_1 \geq \lambda_2 \geq \lambda_3$. Figure 7 shows the PDFs of $\lambda_i \cdot \tau_L$ in various regions conditioned on $c = 0.7$, where $\tau_L$ is the time scale of the reference laminar flame described in Sec. 3.1. It is seen that $\lambda_1$ ($\lambda_2$) is always positive (negative) at plane A. The results are consistent with previous DNS of turbulent premixed flames by Wang *et al.* [27]. From plane A to plane D with increasing wall-normal distance, the contribution of heat release to the strain rate increases [27] and the dilatation $\nabla \cdot \mathbf{u}$ becomes positive. Note that $\nabla \cdot \mathbf{u}$ equals to the sum of the three principal eigenvalues of stain rate tensor, *i.e.* $\nabla \cdot \mathbf{u} = \lambda_1 + \lambda_2 + \lambda_3$. It can be seen that the main contribution of $\nabla \cdot \mathbf{u}$ is $\lambda_1$ at plane D, as expected for laminar premixed combustion.

The interactions of turbulence and reaction fronts are examined with

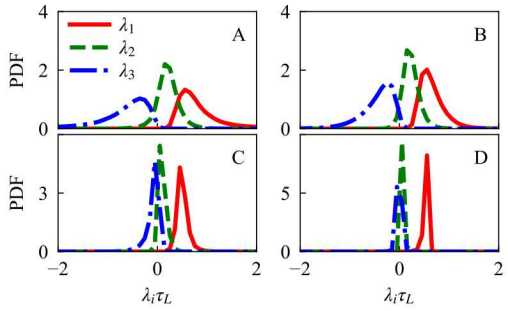


Figure 7: The PDFs of principal eigenvalues of the strain rate tensor in various regions conditioned on $c = 0.7$.

respect to the alignments between the front normal vector $\mathbf{n}$ and the strain rate eigenvectors $\mathbf{e}_i$, which is denoted as $|\mathbf{n} \cdot \mathbf{e}_i|$. The PDFs of $|\mathbf{n} \cdot \mathbf{e}_i|$ in various regions conditioned on $c = 0.02$, 0.7 and 0.95 are presented in Fig. 8. As can be seen, the front normal $\mathbf{n}$ preferentially aligns with the most compressive strain rate $\mathbf{e}_3$ at planes A and B on $c = 0.02$ and 0.95 and plane C on $c = 0.02$, where the effect of heat release on flow straining is small [27, 28]. In contrast, the flame normal aligns with the most extensive strain rate at planes C and D on $c = 0.70$ and 0.95, with an increasing role of heat release rate on the strain rate [29].

### *3.3. Interactions of wall and combustion*

Improved understanding of flame-wall interactions is required for advanced modeling and design of practical combustion devices. The local flame quenching and wall heat flux attract considerable research interest due to their potential impacts on combustion efficiency and safety. In previous work of laminar flames, the local quenching phenomenon was investigated using two parameters, *i.e.* the quenching distance $\delta_Q$ and the corre-

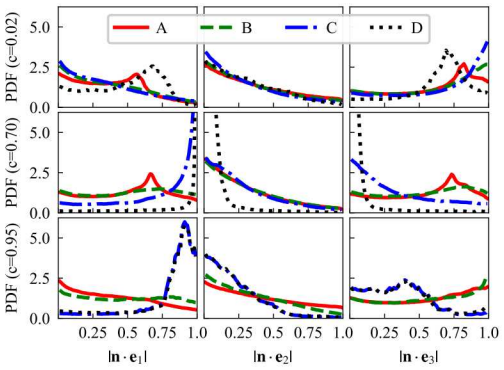


Figure 8: The PDFs of $|\mathbf{n} \cdot \mathbf{e}_i|$ in various regions conditioned on $c = 0.02$, 0.70 and 0.95.

sponding wall heat flux $\Phi_Q$. The quenching Peclet number, $P_q$, is defined as the quenching distance normalized by the premixed flame thickness $\delta_L$, *i.e.* $Pe_Q = \delta_Q/\delta_L$, and the normalized wall heat flux, $\tilde{Q}|_w$, is defined as $\tilde{Q}|_w = \Phi_Q/(\rho_u S_l c_p(T_2 - T_1))$, where $\rho_u$ is the reactant density, $S_l$ is the laminar flame speed, $c_p$ is the specific heat capacity, and $T_2$ and $T_1$ are the temperature of the products and reactants, respectively, of a laminar premixed flame with $T_1 = T_w$ and composition from the DNS (this choice is justified as flame quenching occurs in the near-wall region). In the present work, the flame-wall interactions are significantly influenced by turbulence, and head-on quenching (HOQ), side-wall quenching (SWQ) and oblique-wall quenching (OWQ) occur simultaneously. The identification of flame quenching edges can be problematic. Here, we define the edges of flame quenching as the intersection of the iso-surfaces $c = 0.7$ and $T = 1100$ K. Sensitivity results of the threshold is provided in the supplemental material.

Figure 9 shows the joint PDF of $Pe_Q$ and $\tilde{Q}|_w$ of flame quenching edges. It can be seen that $\tilde{Q}|_w$ is inversely proportional to $Pe_Q$, which is in good

agreement with the trend observed in previous work [2, 3, 30]. Two additional simulations of one-dimensional HOQ are performed to further explain the observations. In the first simulation (denoted as 1D-HOQ-A), the initial temperature profile is set to the mean temperature profile in the wall-normal direction of the DNS. In this case, auto-ignition occurs in high temperature regions away from the wall and then the ignition front propagates towards the wall, quenching at $y = \delta_Q$. In the second simulation (denoted as 1D-HOQ-B), a one-dimensional laminar unstrained premixed flame with $T_1 = 750$ K is used to initialize the calculation, which propagates towards the wall and quenches at $y = \delta_Q$. The results of the two simulations are superimposed in Fig. 9. It is readily observed that the one-dimensional simulation results agree with the DNS results reasonably well.

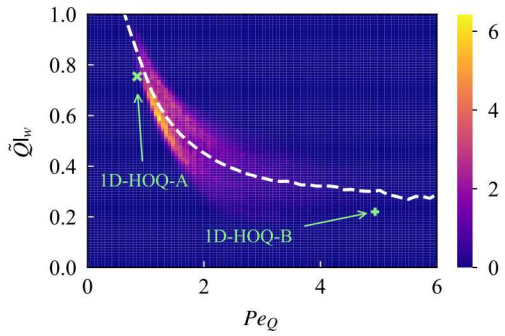


Figure 9: The joint PDF of $Pe_Q$ and $\tilde{Q}|_w$. The white dashed line represents conditional mean. The markers denote results from one-dimensional simulations.

Previous studies suggested that the local quenching phenomenon could be understood with simple chemistry [2, 31–33], and reactions in the quenching distance were neglected. However, it was found by Gruber *et al.* [4] that reactions of intermediate species contribute to heat release in the near-wall

region. In the present work, significant heat release at the wall is also observed intermittently, depending on the angle between the flame normal $\mathbf{n}$ and the wall normal $\mathbf{n_w}$, which is measured with the quantity $\mathbf{n} \cdot \mathbf{n}_w$. The relationship of $\mathbf{n} \cdot \mathbf{n}_w = 1$ implies that the flame is propagating away from the wall, which is named as back-on quenching (BOQ) in the present work, $\mathbf{n} \cdot \mathbf{n}_w = -1$ indicates HOQ, $\mathbf{n} \cdot \mathbf{n}_w = 0$ indicates SWQ, and other values of $\mathbf{n} \cdot \mathbf{n}_w$ indicates OWQ. Figure 10 shows a typical snapshot for HOQ and BOQ. In Fig. 11a, the heat release rate at the wall conditioned on $\mathbf{n} \cdot \mathbf{n}_w$ and various $c$ iso-surfaces is displayed. As can be seen, the heat release rate is negatively correlated with $\mathbf{n} \cdot \mathbf{n}_w$. It can therefore be concluded that the heat release rate at the wall is the highest when HOQ occurs and the lowest heat release rate is observed in BOQ.

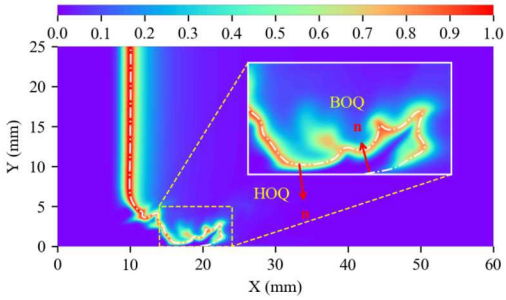


Figure 10: Instantaneous snapshot of HOQ and BOQ. The contours show normalized HRR, and red arrows denote flame normal. The white dash-dotted line denotes the location of $c = 0.7$.

The heat release rate for various elementary reactions is also analyzed. It is found that three reactions, *i.e.* $O_2 + H\ (+M) \Leftrightarrow HO_2\ (+M)$ (R9), $H + HO_2 \Leftrightarrow 2OH$ (R11) and $OH + H\ (+M) \Leftrightarrow H_2O\ (+M)$ (R8), contribute to most of the heat. Similar trends were observed by Gruber *et al.* [4]. Figure 11b shows the heat

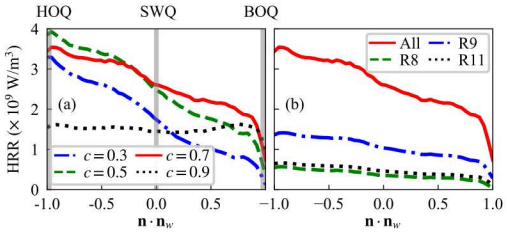


Figure 11: Heat release rate conditioned on $\mathbf{n} \cdot \mathbf{n}_w$ and (a) various iso-surfaces of $c$ and (b) various elementary reactions on $c = 0.7$.

release rate of various elementary reactions conditioned on $\mathbf{n} \cdot \mathbf{n}_w$ and $c = 0.7$. Again, the heat release from elementary reactions decreases with increasing value of $\mathbf{n} \cdot \mathbf{n}_w$.

## 4. Conclusions

A DNS study of premixed combustion in boundary layer turbulence under auto-ignitive conditions is conducted in the present work. The inflow of the reactive DNS is provided by an auxiliary inert DNS of turbulent boundary layer, which has been validated against existing data in the literature. The reactants of the DNS are lean mixtures with a high temperature and a short ignition delay. The main findings of this work are summarized as follows. *First*, the complex combustion modes of auto-ignition and flame propagation are revealed based on the analyses of displacement velocity and species budget. It was found that the reaction front in the free-stream is stabilized by auto-ignition and flame propagation plays an increasingly important role as the wall-normal distance decreases. *Second*, the contribution of heat release to the strain rate increases with increasing wall-normal distance, which has considerable effects on the alignment characteristics between the flame

normal vector and strain rate tensor. *Finally*, the flame-wall interactions are examined and it was found that the wall heat flux is inversely proportional to the flame quenching distance. Heat release at the wall is evident; the highest heat release corresponds to head-on quenching while the lowest heat release corresponds to back-on quenching. These findings are helpful to establish advance models for flame-wall interactions which will be explored in future work.

## Acknowledgments

This work was supported by Natural Science Foundation of China (Grant No.: 51836007) and the Fundamental Research Funds for the Central Universities.

## References

[1] A. Dreizler, B. Böhm. Advanced laser diagnostics for an improved understanding of premixed flame-wall interactions. Proc. Combust. Inst. 35 (1) (2015) 37–64.

[2] T. Poinsot, D. C. Haworth, G. Bruneaux. Direct simulation and modeling of flame-wall interaction for premixed turbulent combustion. Combust. Flame 95 (1-2) (1993) 118–132.

[3] G. Bruneaux, K. Akselvoll, T. Poinsot, J. Ferziger. Flame-wall interaction simulation in a turbulent channel flow. Combust. Flame 107 (1-2) (1996) 27–44.

[4] A. Gruber, R. Sankaran, E. Hawkes, J. Chen. Turbulent flame–wall interaction: a direct numerical simulation study. J. Fluid Mech. 658 (2010) 5–32.

[5] A. Gruber, J. H. Chen, D. Valiev, C. K. Law. Direct numerical simulation of premixed flame boundary layer flashback in turbulent channel flow. J. Fluid Mech. 709 (2012) 516–542.

[6] J. Lai, N. Chakraborty, P. Zhao, L. Wang. Heat flux and flow topology statistics in oblique and head-on quenching of turbulent premixed flames by isothermal inert walls. Combust. Sci. Tech. 191 (2) (2019) 353–381.

[7] Z. Pouransari, L. Biferale, A. V. Johansson. Statistical analysis of the velocity and scalar fields in reacting turbulent wall-jets. Phys. Fluids 27 (2) (2015) 025102.

[8] Y. Wang, A. Trouvé. Direct numerical simulation of nonpremixed flame–wall interactions. Combust. Flame 144 (3) (2006) 461–475.

[9] F. Güthe, J. Hellat, P. Flohr. The reheat concept: the proven pathway to ultralow emissions and high efficiency and flexibility. J. Eng. Gas Turbine Power 131 (2) (2009) 021503.

[10] J. M. Fleck, P. Griebel, A. M. Steinberg, C. M. Arndt, C. Naumann, M. Aigner. Autoignition of hydrogen/nitrogen jets in vitiated air cross-flows at different pressures. Proc. Combust. Inst. 34 (2) (2013) 3185–3192.

[11] O. Schulz, N. Noiray. Combustion regimes in sequential combustors:

Flame propagation and autoignition at elevated temperature and pressure. Combust. Flame 205 (2019) 253–268.

[12] K. Aditya, A. Gruber, C. Xu, T. Lu, A. Krisman, M. R. Bothien, J. H. Chen. Direct numerical simulation of flame stabilization assisted by autoignition in a reheat gas turbine combustor. Proc. Combust. Inst. 37 (2) (2019) 2635–2642.

[13] J. A. Wagner, S. W. Grib, M. W. Renfro, B. M. Cetegen. Flowfield measurements and flame stabilization of a premixed reacting jet in vitiated crossflow. Combust. Flame 162 (10) (2015) 3711–3727.

[14] D. A. Pennell, M. R. Bothien, A. Ciani, V. Granet, G. Singla, S. Thorpe, A. Wickstroem, K. Oumejjoud, M. Yaquinto. An introduction to the Ansaldo GT36 constant pressure sequential combustor. In ASME Turbo Expo 2017: Turbomachinery Technical Conference and Exposition. American Society of Mechanical Engineers (2017) pp. V04BT04A043–V04BT04A043.

[15] J. Li, Z. Zhao, A. Kazakov, F. L. Dryer. An updated comprehensive kinetic model of hydrogen combustion. Int. J. Chem. Kinet. 36 (10) (2004) 566–575.

[16] P. Schlatter, R. Örlü. Assessment of direct numerical simulation data of turbulent boundary layers. J. Fluid Mech. 659 (2010) 116–126.

[17] M. Morkovin. Compressible effects on turbulence. Mécanique de la Turbulence. CNRS Press, France .

[18] E. R. Van Driest. Turbulent boundary layer in compressible fluids. Journal of spacecraft and rockets 40 (6) (2003) 1012–1028.

[19] S. Pirozzoli, M. Bernardini. Turbulence in supersonic boundary layers at moderate Reynolds number. J. Fluid Mech. 688 (2011) 120–168.

[20] J. H. Chen, A. Choudhary, B. De Supinski, M. DeVries, E. R. Hawkes, S. Klasky, W.-K. Liao, K.-L. Ma, J. Mellor-Crummey, N. Podhorszki, et al. Terascale direct numerical simulations of turbulent combustion using S3D. Comput. Sci. Discovery. 2 (1) (2009) 015001.

[21] C. A. Kennedy, M. H. Carpenter. Several new numerical methods for compressible shear-layer simulations. Appl. Numer. Math. 14 (4) (1994) 397–433.

[22] H. Wang, E. R. Hawkes, J. H. Chen. A direct numerical simulation study of flame structure and stabilization of an experimental high Ka CH4/air premixed jet flame. Combust. Flame 180 (2017) 110–123.

[23] S. Pope. The evolution of surfaces in turbulence. Int. J. Eng. Sci. 26 (5) (1988) 445–469.

[24] T. Echekki, J. H. Chen. Analysis of the contribution of curvature to premixed flame propagation. Combust. Flame 118 (1-2).

[25] H. G. Im, J. H. Chen. Preferential diffusion effects on the burning rate of interacting turbulent premixed hydrogen-air flames. Combust. Flame 131 (3) (2002) 246–258.

[26] A. Krisman, E. R. Hawkes, J. H. Chen. The structure and propagation of laminar flames under autoignitive conditions. Combust. Flame 188 (2018) 399–411.

[27] H. Wang, E. R. Hawkes, J. H. Chen. Turbulence-flame interactions in DNS of a laboratory high Karlovitz premixed turbulent jet flame. Phys. Fluids 28 (9) (2016) 095107.

[28] W. T. Ashurst, A. Kerstein, R. Kerr, C. Gibson. Alignment of vorticity and scalar gradient with strain rate in simulated Navier–Stokes turbulence. The Phys. Fluids 30 (8) (1987) 2343–2353.

[29] N. Chakraborty, M. Klein, N. Swaminathan. Effects of Lewis number on the reactive scalar gradient alignment with local strain rate in turbulent premixed flames. Proc. Combust. Inst. 32 (1) (2009) 1409–1417.

[30] F. Dabireau, B. Cuenot, O. Vermorel, T. Poinsot. Interaction of flames of H2+ O2 with inert walls. Combust. Flame 135 (1-2) (2003) 123–133.

[31] C. K. Westbrook, A. A. Adamczyk, G. A. Lavoie. A numerical study of laminar flame wall quenching. Combust. Flame 40 (1981) 81–99.

[32] J. Lai, N. Chakraborty. Effects of Lewis number on head on quenching of turbulent premixed flames: a direct numerical simulation analysis. Flow Turbul. Combust. 96 (2) (2016) 279–308.

[33] J. Sellmann, J. Lai, A. M. Kempf, N. Chakraborty. Flame surface density based modelling of head-on quenching of turbulent premixed flames. Proc. Combust. Inst. 36 (2) (2017) 1817–1825.